Inorganic Chemistry
Cite This: Inorg. Chem. 2018, 57, 10568−10575
Article
pubs.acs.org/IC

$ALiZnP_2O_7$ (A = Rb, Cs): Two Mixed Alkali Zinc Pyrophosphates Featuring a $[Li_2Zn_2P_4O_{20}]^{14-}$ Anionic Skeleton

Zhaohui Chen,*[,†,‡] Yuan Fang,[†,‡] Wenyao Zhang,[†] Wenqiang Chen,[†] Xuefang Lu,[†] Qun Jing,*[,†] and Ming-Hsien Lee[§]

[†]Physical and Chemical Detecting Center, College of Chemistry and Chemical Engineering, and School of Physical Science and Technology, Xinjiang University, 666 Shengli Road, Urumqi 830046, China

[§]Department of Physics, Tamkang University, New Taipei City 25137, Taiwan

Supporting Information

ABSTRACT: Two new isotypic diphosphates, $RbLiZnP_2O_7$ (RLZP) and $CsLiZnP_2O_7$ (CLZP), have been synthesized by a high-temperature solid-phase method. They both crystallize in the *Pnma* space group (No. 62) and have similar crystal configurations. $ALiZnP_2O_7$ (A = Rb, Cs) consists of a $[Li_2Zn_2P_4O_{20}]^{14-}$ anionic skeleton, which is composed of Li/ZnO_4 tetrahedral and diphosphate groups, and the Rb or Cs atoms are located in the large hole. In this paper, we discuss the structures of the title compounds and isonomic $AA'ZnP_2O_7$ (A = alkali metal); it is found that the ionic radii of the cations and bond angles have an effect on the symmetry of the compounds. By analysis, we found that the M/P values have some effect on the dimensionality of the anionic groups in phosphates containing P_2O_7 groups. Thermal and spectral analyses are carried out on the title compounds. Besides that mentioned above, we also studied the relationship between the electronic structures and optical properties by theoretical calculations.

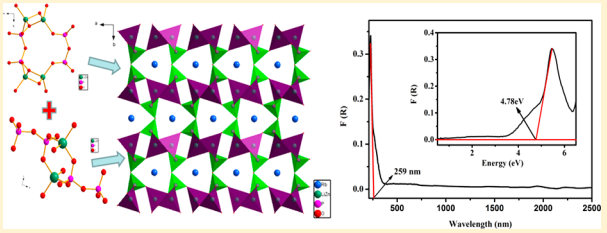

INTRODUCTION

Phosphates can be widely applied in various fields, such as ceramic, ferroelectric, electric, light-emitting diodes (LEDs), catalytic materials, nonlinear-optical (NLO) materials, and so on.[1] For example, KH_2PO_4 and $KTiOPO_4$ can be used in laser frequency conversion; $LiFePO_4$ and $Li_3V_2(PO_4)_3$ are mature lithium battery materials.[2] $ABPO_4:Eu^{2+}$ (A = alkali metals and B = alkaline-earth metals) are applied to LEDs as a new system.[3]

Owing to varied types of polymerization for $[PO_4]^{3-}$ groups, phosphate can be classified into different categories, such as isolated $[PO_4]^{3-}$, $[P_2O_7]^{4-}$ dimer, and isolated $[P_nO_{3n+1}]^{(n+2)-}$, ringed $[P_nO_{3n}]^{n-}$, or straight chain $(PO_3)_\infty$ for $n \geq 3$ groups.[4] In recent years, phosphates have drawn enough attention for exploring and designing new ultraviolet (UV) or deep-UV NLO materials since Chen's group reported the $Ba_3P_3O_{10}X$ (X = Cl, Br) compounds.[5]

In order to explore deep-UV NLO materials, many researchers combined the first and second main-group metals or some rare-earth metals with phosphates, owing to the lack of d−f electron transitions in these metal cations.[6] Under the guidance of this design, many NLO phosphates were discovered, such as $LiCs_2PO_4$, $RbBa_2(PO_3)_5$, $Ba_5P_6O_{20}$, $RbBa_2(PO_3)_5$, $Rb_2Ba_3(P_2O_7)_2$, $KLa(PO_3)_4$, $RbNaMgP_2O_7$, $CsNaMgP_2O_7$, and so on.[7] Besides outstanding performances, there are some excellent structural compounds, such as $A_3Sr_2P_7O_{21}$ (A = Rb, Cs), $Cs_2MgZn_2(P_2O_7)_2$, and $Pb_{12}[Li_2(P_2O_7)_2(P_4O_{13})_2](P_4O_{13})$.[8] These compounds are rich in structural types and functional properties.

Generally, Zn atoms can form ZnO_4, ZnO_5, or ZnO_6 polyhedra coordination environments, which can enrich the crystal structures as fundamental building units. Because of its rich structure and diverse functional properties, a large number of alkali zinc diphosphates were discovered, for instance, $Na_2ZnP_2O_7$, $K_2ZnP_2O_7$, $LiNaZnP_2O_7$, $LiKZnP_2O_7$, $NaKZnP_2O_7$ (NKZP), $Li_{12}Zn_4(P_2O_7)_5$, $K_2Zn_3(P_2O_7)_2$, etc.[9] In view of these advantages of phosphates, we banded together alkali-metal, zinc, and phosphate groups and expected to get compounds with novel crystal structures and excellent optical performances. By exploring the $A_2O-ZnO-P_2O_5$ (A = alkali metal) system, we synthesized two new compounds, $RbLiZnP_2O_7$ (RLZP) and $CsLiZnP_2O_7$ (CLZP). In this paper, we discuss the structures of $AA'ZnP_2O_7$ (A = alkali metal) compounds,[10] and only $KLiZnP_2O_7$ (KLZP) crystallizes in the noncentrosymmetric (NCS) space group. By a structural comparison, we analyze the causes of why these compounds crystallize in different space groups. In addition, the effects of cationic radii on crystal configurations are discussed in detail.

Further studies include a crystal structure comparison, thermal analysis, and relevant spectroscopic measurements. Besides, first-principles calculations are used to evaluate the roles of different orbital hybrid states for the electron band gaps.

Received: April 25, 2018
Published: August 20, 2018

DOI: 10.1021/acs.inorgchem.8b01140
Inorg. Chem. 2018, 57, 10568−10575

EXPERIMENTAL SECTION

Solid-State Synthesis. We synthesized polycrystalline RLZP and CLZP by high-temperature solid-state reactions with Rb_2CO_3 (Cs_2CO_3 for CLZP, Aladdin, 99.8%), Li_2CO_3 (Aladdin, 99%), ZnO (Aladdin, 99.5%), and $NH_4H_2PO_4$ (Aladdin, 98%). The reactants are mixed by a stoichiometric ratio, ground thoroughly in an agate mortar, and then slowly heated to 450 °C at a rate of 1 °C min^{-1} to avoid spraying reactants owing to volatilization of CO_2 and NH_3. Then the mixtures were sintered at 700 °C (RLZP) and 720 °C (CLZP), respectively, and held for 3 days. The mixtures were ground several times during the period. The powder X-ray diffraction (XRD) patterns were recorded on a Bruker D2 X-ray diffractometer with Cu Kα radiation (λ = 1.5418 Å) in the 2θ range from 10° to 70° with a step size of 0.02° and a fixed counting time of 1 s $step^{-1}$ (Figure S1). The experimental XRD patterns of RLZP and CLZP are consistent with the calculated ones based on single-crystal structure data.

Crystal Growth. Single crystals of RLZP and CLZP were obtained by a high-temperature solution method in the $A_2O-ZnO-P_2O_5$ (A = alkali metal) system. To RLZP, Rb_2CO_3, Li_2CO_3, ZnO, and $NH_4H_2PO_4$ at molar ratios of 3:5:5:10 were mixed, ground thoroughly, and then transferred into a platinum crucible. The crucible was put into a single-crystal growth furnace and then heated to 760 °C for 12 h. The solution was gradually cooled to 700 °C at 2 °C h^{-1} and then rapidly reduced to 500 °C at a rate of 20 °C h^{-1}. The semisolid melt was cooled to 30 °C at 50 °C h^{-1}. Colorless block crystals were obtained successfully. We took the platinum crucible out of the single-crystal growth furnace and observes the block crystals on the surface of the crucible, which were detached from the crucible. Crystals of CLZP were obtained under a similar process.

Single-Crystal X-ray Diffraction. Two colorless block crystals of RLZP and CLZP were picked for the collection of single-crystal data (Figure S2). A Bruker Smart APEX II single-crystal diffractometer was used to collect diffraction data. The reductions of data were carried out with the Bruker Suite software package. Multiscan absorption corrections were performed with the *SADABS* program.[11] The structures were solved by direct methods and refined by the full-matrix least-squares method with anisotropic displacement parameters in the *SHELXL-97* system.[12] They were checked with the aid of the program *PLATON*,[13] and no higher symmetries were recommended. Details of the crystal parameters, data collection, and structure refinement are given in Table 1. Atomic coordinates and isotropic or equivalent displacement parameters are summarized in Tables S1 and S2. The main interatomic distances and angles are given in Tables S3 and S4.

IR Spectra. IR spectra were measured on a Shimadzu IR Affinity-1 Fourier transform infrared spectrometer in the range of 400−4000 cm^{-1}. RLZP and CLZP compounds were mingled fully with dried KBr according to the 1:20 ratio, respectively.

UV−Vis−Near-IR (NIR) Diffuse-Reflectance Spectroscopy. The UV−vis−NIR diffuse-reflectance spectra were collected with a Shimadzu SolidSpec-3700DUV spectrophotometer from 190 to 2600 nm.

Thermal Behavior Analysis. Thermal gravimetric (TG) and differential scanning calorimetry (DSC) analyses were carried out on a Hitachi STA 7300 thermal analyzer instrument with a flowing argon atmosphere. The RLZP and CLZP compounds (5−10 mg) were heated from 30 to 1000 °C at a rate of 5 °C min^{-1} in a Al_2O_3 crucible, respectively.

Theoretical Calculations. The electronic structures and optical properties of the title compounds were calculated using the *CASTEP* package.[14] As shown in the CIF files for RLZP (CLZP), one independent metal position is half-occupied by the Li and Zn atoms in its asymmetric unit. The half-occupied Li/Zn atoms were found at different layers (shown in layers 1−3 in Figure 1). To better understand the electronic structures and optical properties of these compounds, several different models with separated Li and Zn atoms are used. The separated Li and Zn atoms either sit in different layers (marked as hyp04 in Figures 2 and S3) or sit in the same layer but with different sequences (marked as hyp01, hyp02, and hyp03 in Figures 2 and S3). The differences among the models hyp01, hyp02, and hyp03 are the sequences of Li and Zn atoms: the Li and Zn atoms are separated with another kind of atom (Li, Zn, Li, and Zn in layer 2; marked as hyp01), the Li atom is far away from the Li atom, but the Zn atom is neighbors with the Zn atom (Li, Zn, Zn, and Li in layer 2; marked as hyp03), and the Li/Zn atoms are neighbors with the same kind of Li/Zn atoms (Li, Li, Zn, and Zn in layer 2; marked as hyp02). The authors made detailed investigations on the electronic structures and optical properties of compounds with different arrangements of Li/Zn atoms. During the calculations, the generalized gradient approximation with the Perdew−Burke−Ernzerhof functional was adopted.[15] Under the norm-conserving pseudopotential, the following orbital electrons were treated as valence electrons: Li, $2s^1$; O, $2s^22p^4$; P, $3s^23p^3$; Zn, $3d^{10}4s^2$; Rb, $4s^24p^65s^1$; Cs, $5s^25p^66s^1$. A kinetic energy cutoff of 830 eV was chosen, and the numerical integration of the Brillouin zone was performed using a 2 × 2 × 5 Monkhorst−Pack *k*-point sampling. The other calculation parameters and convergent criteria were the default values of the *CASTEP* code.

Table 1. Crystal Data and Structure Refinement for RLZP and CLZP

empirical formula	$RbLiZnP_2O_7$	$CsLiZnP_2O_7$
fw	331.72	379.16
temperature (K)	296(2)	
wavelength (Å)	0.71073	
cryst syst, space group	orthorhombic, *Pnma*	
unit cell dimens		
a (Å)	10.4283(10)	10.6327(11)
b (Å)	12.3858(11)	12.3172(13)
c (Å)	5.1193(5)	5.2048(5)
volume ($Å^3$)	661.22 (11)	681.65 (11)
Z, calcd density (g cm^{-3})	4, 3.325	4, 3.695
abs coeff (mm^{-1})	11.445	9.324
F(000)	623	696
cryst size (mm^3)	0.20 × 0.15 × 0.1	0.20 × 0.15 × 0.1
θ range for data collection (deg)	3.91−27.50	3.31−27.57
limiting indices	$-12 \le h \le 13$, $-9 \le k \le 16$, $-5 \le l \le 6$	$-13 \le h \le 9$, $-15 \le k \le 15$, $-6 \le l \le 6$
reflns collected/unique	3653/787 [*R*(int) = 0.0327]	4922/820 [*R*(int) = 0.0232]
completeness to θ (%)	99.50	99.50
refinement method	full-matrix least squares on F^2	
data/restraints/param	787/0/60	820/0/60
GOF on F^2	1.079	1.154
final *R* indices [$I > 2\sigma(I)$][a]	R_1 = 0.0233, wR_2 = 0.0582	R_1 = 0.0154, wR_2 = 0.0412
R indices (all data)[a]	R_1 = 0.0279, wR_2 = 0.0598	R_1 = 0.0158, wR_2 = 0.0414
extinction coeff	0.0121(10)	0.0455(11)
largest diff peak and hole (e $Å^{-3}$)	0.457 and −0.534	0.702 and −0.473

[a] $R_1 = \sum||F_o| - |F_c||/\sum|F_o|$ and $wR_2 = [\sum w(F_o^2 - F_c^2)^2/\sum wF_o^4]^{1/2}$ for $F_o^2 > 2\sigma(F_o^2)$.

RESULTS AND DISCUSSION

Crystal Structure. By analysis of the crystal structures, we know that RLZP and CLZP are isotypic and in the same space group *Pnma* (Figures 3 and S4). Hence, we take RLZP as an example to discuss elaborately. Its basic units include a Rb atom, a independent position occupied by half each of the Li and Zn atoms, a P atom, and four O atoms. The RLZP crystal structure presents a three-dimensional (3D) framework formed

DOI: 10.1021/acs.inorgchem.8b01140
Inorg. Chem. 2018, 57, 10568−10575

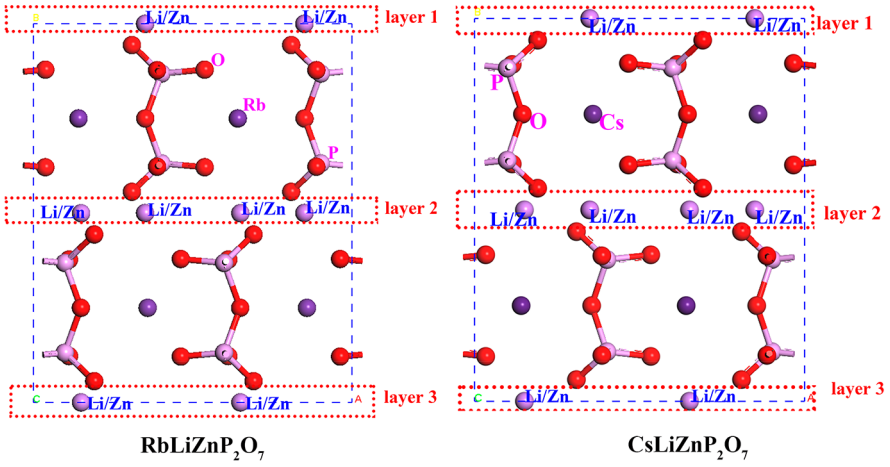

Figure 1. Crystal structures of the RLZP and CLZP compounds. The red, dark orchid, and violet balls represent the O, Rb, and P atoms; the Li/Zn atoms are marked with blue characters.

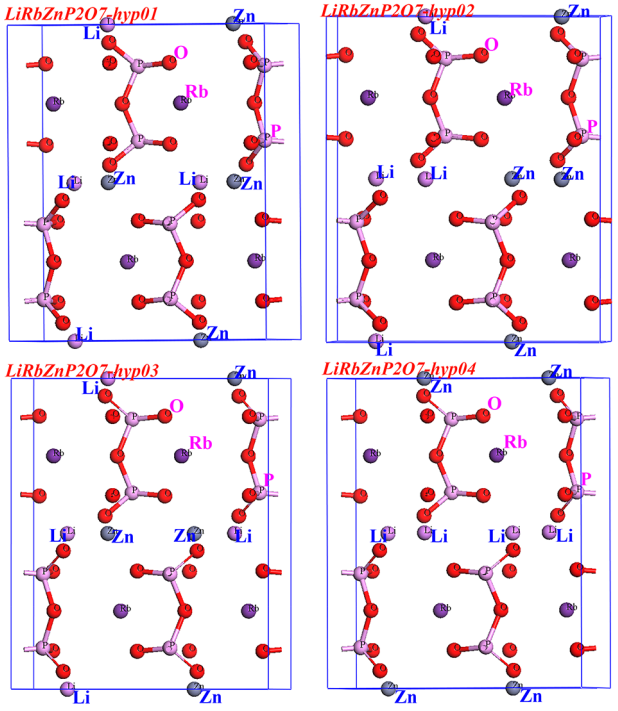

Figure 2. Models of RLZP used for first-principles calculations. The red, dark orchid, and violet balls represent the O, Rb, and P atoms; the Li/Zn atoms are marked with blue characters.

by isolated P_2O_7, Li/ZnO_4, and RbO_{12} units. All P atoms form PO_4 tetrahedra with O atoms in the structures of RLZP and CLZP and then form P_2O_7 groups. The P_2O_7 units interconnect to build AA′AA′ pseudolayer arrangements, and the P_2O_7 groups of the A and A′ layers are in the opposite directions (Figure 3a) with the P−O bond lengths between 1.5071(18) and 1.616(11) Å. In the crystal structure, a new anionic group, $[Li_2Zn_2P_4O_{20}]^{14-}$, is composed of two P_2O_7 double clusters and four disordered Li/ZnO_4 groups. The adjacent groups along the *a* axis interconnect with each other by Li/ZnO_4 terminus O atoms, and the upper and lower repeating units along the *b* axis are connected by terminal O atoms of the P_2O_7 dimer to construct a tunnel structural framework (Figure 3a), which shows two kinds of tunnels, a wide tunnel forming approximate hexagonal rings filled by the

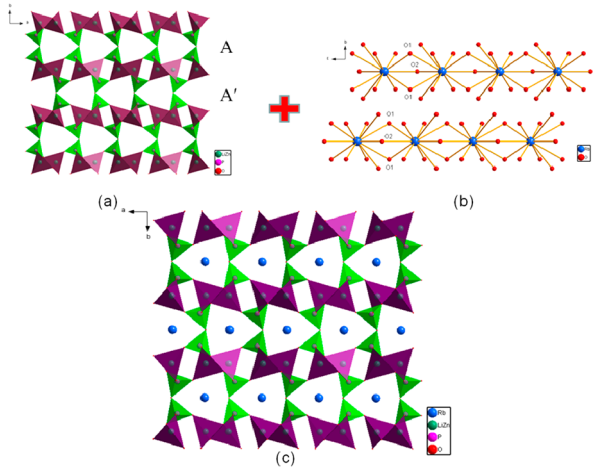

Figure 3. (a) $[Li_2Zn_2P_4O_{20}]^{14-}$ 2D layers. (b) RbO_{12} polyhedra composed of 1D chains. (c) 3D structure of RLZP.

Rb ions and another one showing a rectangle tunnel, respectively. The two kinds of tunnels are observed to interlace and present the opposite arrangement in the adjacent layers, resulting in symmetric and centrosymmetric (CS) structures.

In addition, the Li/Zn and O atoms form Li/ZnO_4 and have bond lengths between 1.912(17) and 1.969(16) Å. Rb atoms are connected with 12 terminal O atoms of the phosphate units with have bond lengths between 2.996(17) and 3.639(2) Å. The neighboring RbO_{12} polyhedra share three O atoms to form a one-dimensional (1D) chain, extending down the *c* axis (Figure 3b).

Crystal Structure Comparison. By investigating the Inorganic Crystal Structure Database (ICSD, http://www2.fizkarlsruhe.de/icsd_web.html), we compared the crystal structures of (a) $NaLiZnP_2O_7$ (NLZP), (b) KLZP, (c) NKZP, (d) RLZP, and (e) CLZP (Figure 4), which share the same formula of AA′ZnP_2O_7 (A = alkali metal), and all form 3D frameworks including separated P_2O_7 groups. It was reported that NLZP crystallized in the *Cmcm* space group. As illustrated in Figure 4a, it consists of isolated P_2O_7, Li/ZnO_4, and NaO_5 units; the repetitive units of the P−O groups are formed by two back-to-back P_2O_7 dimers. Interestingly, the double clusters in NLZP change into single dimers in A$LiZnP_2O_7$ (A = K, Rb, Cs). When the larger K^+ cations

DOI: 10.1021/acs.inorgchem.8b01140
Inorg. Chem. 2018, 57, 10568−10575

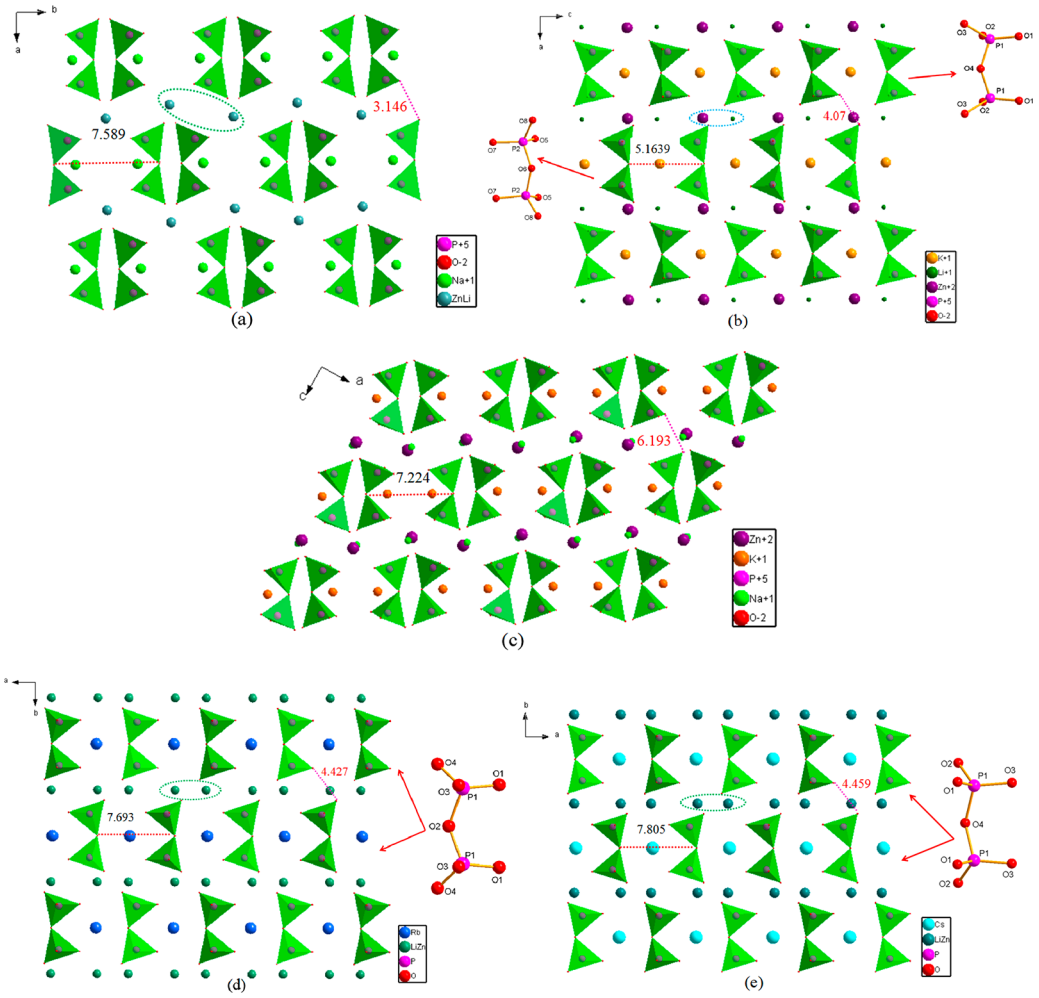

Figure 4. Structural comparison of (a) NLZP, (b) KLZP, (c) NKZP, (d) RLZP, and (e) CLZP. (a and c) Two Na or K atoms filling in the interspace of the back-to-back P_2O_7 dimers. (b) KLZP containing two different orientations of the P_2O_7 groups. (d and e) RLZP and CLZP containing a single orientation of the P_2O_7 group.

replace the Na^+ cations (KLZP), repulsion is produced in the crystal structure of NLZP. Rearrangement of the P_2O_7 groups can reduce the repulsive force to accommodate K^+ cations (Figure 4b). However, the P_2O_7 dimers of NKZP reverse to double-cluster. By a comparison of the interlayer spacing, it is found that the layer spacing of NKZP (6.193 Å) is about 1.5 times KLZP (4.07 Å); that is to say, the repulsion between groups is weakened. The space of the double clusters' arrangement is sufficient to accommodate K^+ cations of NKZP (Figure 4c). Then when K^+ cations of KLZP are substituted by Rb^+ cations, the P_2O_7 units adjust flexibly to free more space to meet the larger radius of the Rb ions. Meanwhile, the P−O−P bond angles in the P_2O_7 groups are also changed, as shown in Figure S5. It can be seen from the analysis that the synergetic effects of the cationic radius and interlayer spacing make a variety of arrangements of the P_2O_7 dimers.

The repulsion between ions brings about the distinction of the bond lengths and bond angles. The distances between anionic groups become larger with an increase in the cationic radius. In RLZP, the upper and lower layers of P_2O_7 just have mutually rotated 180° operations (Figure 4d). However, two different orientations of the P_2O_7 groups of two adjoining layers, including the bond length and bond angle, are presented in KLZP (Figure 4b). The relevant data are listed in Table S5. The dipole moments of the upper and lower layers cannot be completely offset in KLZP. For the above reasons, KLZP and RLZP crystallize in NCS ($Pmc2_1$, No. 26) and CS (*Pnma*, No. 26) space groups correspondingly.

In addition, by screening the ICSD and recent publications, $AA'ZnP_2O_7$ (A = alkali metal) and others containing P_2O_7 group phosphates are compared and analyzed in Table 2.[16] Pan et al. pointed out that the values of M/(B + P) affect the configurations of the anionic groups.[17] Interestingly, there are certain rules in these P_2O_7 group phosphates with increasing M/P values. As can be seen from Table 2, the P−O groups are connected with cationic polyhedra to form groups, and then countless groups exist in isolated zero-dimensional (0D) clusters, 1D chains, two-dimensional (2D) layers, or 3D frameworks. With decreasing M/P ratio, the degree of polymerization of the anionic units tends to change from a complex 3D network to isolated 0D groups. The M/P ratios of the first 16 compounds in Table 2 are 2 or 1.5; the P_2O_7 dimers and the cationic polyhedra are interconnected to form 2D layers except for $Cs_2BaP_2O_7$ and $CsLiCdP_2O_7$ (3D). When the M/P ratios are between 1.5 and 1.4, the dimensionality of the anionic groups reduces from 2D layers to 1D chains. Especially, when the M/P value is 1.33, the anionic group

DOI: 10.1021/acs.inorgchem.8b01140
Inorg. Chem. 2018, 57, 10568−10575

Table 2. Correlative Phosphates, Their Space Groups, Cation/Phosphorus Ratios (M/P), and Anionic Groups

compound	space group	M/P	anionic group
$LiNa_3P_2O_7$	$C222_1$	2	$^2_\infty[LiP_2O_7]^{3-}$
$LiK_3P_2O_7$	$C222_1$	2	$^2_\infty[LiP_2O_7]^{3-}$
$RbNaMgP_2O_7$	$Ccm2_1$	1.5	$^2_\infty[MgP_2O_7]^{3-}$
$CsNaMgP_2O_7$	$Ccm2_1$	1.5	$^2_\infty[MgP_2O_7]^{3-}$
$Cs_2BaP_2O_7$	$P2_1/n$	1.5	$^3_\infty[BaP_2O_7]^{2-}$
$LiCsBaP_2O_7$	$P2_1/c$	1.5	$^2_\infty[LiP_2O_7]^{3-}$
$Rb_2CdP_2O_7$	$P2_1/c$	1.5	$^2_\infty[CdP_2O_7]^{2-}$
$Cs_2CdP_2O_7$	$Pnma$	1.5	$^2_\infty[CdP_2O_7]^{2-}$
$CsLiCdP_2O_7$	$Pmc2_1$	1.5	$^3_\infty[CdP_2O_7]^{2-}$
$Na_2ZnP_2O_7$	$P4_2/mnm$	1.5	$^2_\infty[ZnP_2O_7]^{2-}$
$K_2ZnP_2O_7$	$P4_2/mnm$	1.5	$^2_\infty[ZnP_2O_7]^{2-}$
$NaLiZnP_2O_7$	$Cmcm$	1.5	$^2_\infty[LiZnP_2O_7]^{-}$
$KLiZnP_2O_7$	$Pmc2_1$	1.5	$^2_\infty[ZnP_2O_7]^{2-}$
$RbLiZnP_2O_7$	$Pnma$	1.5	$^2_\infty[LiZnP_2O_7]^{-}$
$CsLiZnP_2O_7$	$Pnma$	1.5	$^2_\infty[LiZnP_2O_7]^{-}$
$NaKZnP_2O_7$	$P2_1/n$	1.5	$^2_\infty[ZnP_2O_7]^{2-}$
$Na_7Mg_{4.5}(P_2O_7)_4$	$P\bar{1}$	1.44	$^1_\infty[Na_2(P_2O_7)_4]^{14-}$
$Li_{1.52}Na_{4.48}Cd_8(PO_4)_2(P_2O_7)_4$	$P\bar{1}$	1.4	$^1_\infty[M_2P_5O_{20}]^{13-}$(M = Li/Na, Na)
$K_6Bi_2(P_2O_7)_3$	$P1$	1.33	$^3_\infty[Bi_2P_6O_{21}]^{6-}$
$K_4Mg_4(P_2O_7)_3$	Pc	1.33	$^2_\infty[Mg_4P_6O_{21}]^{4-}$
$Rb_4Mg_4(P_2O_7)_3$	$Amm2$	1.33	$^2_\infty[Mg_4P_6O_{21}]^{4-}$
$Pb_9[Li_2(P_2O_7)_2(P_4O_{13})_2]$	$P\bar{1}$	0.92	0D $[Li_2(P_2O_7)_2(P_4O_{13})_2]^{18-}$
$Pb_7Ba_2[Li_2(P_2O_7)_2(P_4O_{13})_2]$	$P\bar{1}$	0.92	0D $[Li_2(P_2O_7)_2(P_4O_{13})_2]^{18-}$
$Pb_3Ba_6[Li_2(P_2O_7)_2(P_4O_{13})_2]$	$P\bar{1}$	0.92	0D $[Li_2(P_2O_7)_2(P_4O_{13})_2]^{18-}$
$Pb_2Ba_7[Li_2(P_2O_7)_2(P_4O_{13})_2]$	$P\bar{1}$	0.92	0D $[Li_2(P_2O_7)_2(P_4O_{13})_2]^{18-}$
$Pb_{12}[Li_2(P_2O_7)_2(P_4O_{13})_2](P_4O_{13})$	$P\bar{1}$	0.88	0D $[Li_2(P_2O_7)_2(P_4O_{13})_2]^{18-}$

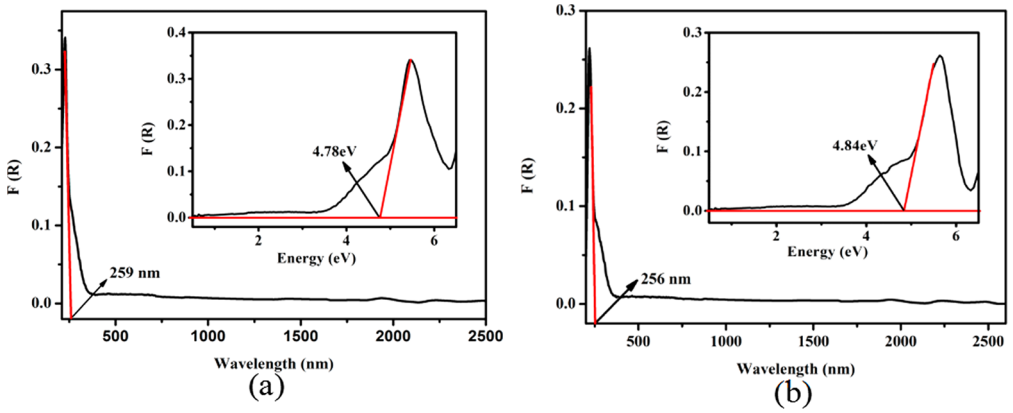

Figure 5. UV−vis−NIR diffuse-reflectance spectra of (a) RLZP and (b) CLZP.

Table 3. Obtained Band Gaps of RLZP and CLZP with Different Arrangements of Li/Zn Atoms (Shown in Figures 1 and S3)

	RLZP				CLZP			
	hyp01	hyp02	hyp03	hyp04	hyp01	hyp02	hyp03	hyp04
band gap (eV)	3.31	2.78	3.08	0.37	3.34	2.83	3.19	0.73

reverses from 1D chains to 2D layers and 3D frameworks. We conjecture that a M/P value of 1.33 is a demarcation point for phosphates containing P_2O_7 groups and runs counter to the above-mentioned rule, and the special cases need to be further studied. When the M/P ratio is less than 1, we observed two trends: (1) the anionic groups change to isolated groups; (2) the phosphates have two or three kinds of discrete P−O groups. On the basis of analysis, the general trend can be summarized as lower values of M/P correspond to lower dimensionalities of P−O groups. Guided by the above analysis, we may design phosphates with abundant structure types by adjusting the M/P ratio.

IR Spectra. To further confirm the coordination of phosphates in $ALiZnP_2O_7$ (A = Rb, Cs), IR spectra are shown in Figure S6 and both compounds yield similar spectra. The bands near 900 and 1190 cm^{-1} can be derived from the bridge P−O−P vibrations. Then the peaks around 700 and 600 cm^{-1} can be related to P−O symmetric and asymmetric

DOI: 10.1021/acs.inorgchem.8b01140
Inorg. Chem. 2018, 57, 10568−10575

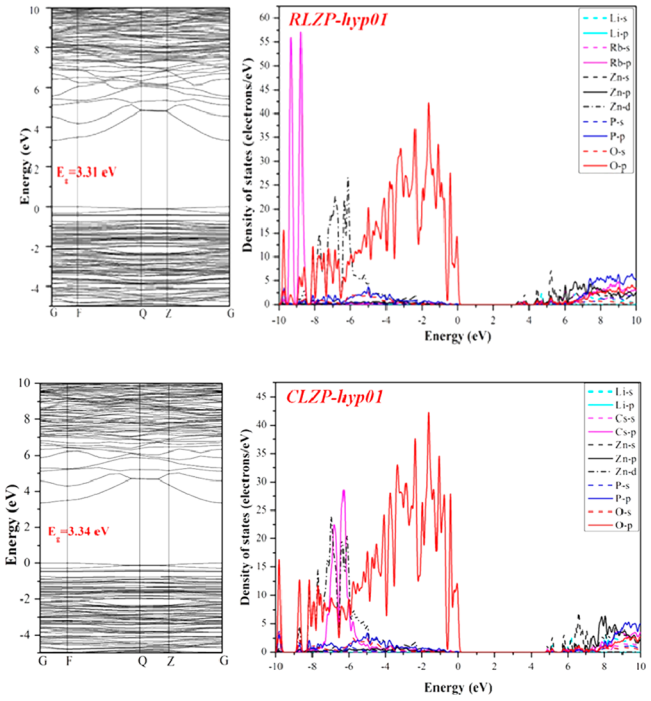

Figure 6. Obtained band structures and projected density of states of RLZP-hyp01 (upper panel) and CLZP-hyp01 (lower panel).

stretching in P−O−P. The absorption peaks about 500 cm^{-1} are attributed to the base frequency of the PO_4 groups. The results of the IR spectra coincide with the P−O groups of the $ALiZnP_2O_7$ (A = Rb, Cs) compounds.

Thermal Behaviors. The TG−DSC curves of RLZP and CLZP indicate that they are stable and without weight loss below 900 °C (Figure S7). On the DSC curves, two sharp endothermic peaks were observed at 805 and 825 °C for RLZP and CLZP, respectively, and the two thermopositive peaks, at 785 and 772 °C, on the cooling curve for RLZP and CLZP, respectively. We preliminarily infer that both of the compounds have congruent melting. To verify the conclusion, we carried out powder XRD analysis on the title compounds before and after melting (Figure S1). The powder XRD curves of the before- and after-melting compounds are both consistent with those simulated from single-crystal structures, which indicate that RLZP and CLZP have congruent melting.

UV−Vis−NIR Diffuse-Reflectance Spectra. The spectra were conducted on the RLZP and CLZP crystals (Figure 5). From the curves, we can see that the cutoff edges of the reported compounds are around 260 nm. We calculated absorption data according to the Kubelka−Munk function.[18] For the linear part of the ascending curve, the extrapolation method provides two onsets of absorption at 4.78 eV (RLZP) and 4.84 eV (CLZP).

Electronic Structures and Optical Properties. Using the calculations technique represented in the Experimental Section, we studied the electronic structures and optical performances of RLZP and CLZP. The obtained band gaps of RLZP and CLZP with different arrangements of the Li/Zn atoms are given in Table 3. The theoretical band gaps of RLZP and CLZP (3.31 eV for RLZP-hyp01, and 3.34 eV for CLZP-hyp01) are smaller than those of the experimental (4.78 and 4.84 eV) results, which are consistent with the reported compounds.[8] Furthermore, the obtained band gaps of RLZP-hyp01, RLZP-hyp02, RLZP-hyp03, CLZP-hyp01, CLZP-hyp02, and CLZP-hyp03 are similar to the experimental values, while the obtained band gaps of RLZP-hyp04 and CLZP-hyp04 are much smaller than the experimental values, indicating that the Li/Zn atoms may be arranged alternately in the Li/Zn layers in the compounds (shown in Figures 2 and S3). Among these model structures, RLZP-hyp01 and CLZP-hyp01 own the smallest error between the calculated and experimental band gaps; hence, the authors would further investigate the RLZP-hyp01 and CLZP-hyp01 models.

As shown in Figure 6, RLZP-hyp01 and CLZP-hyp01 own similar band structures. They are both direct-band-gap compounds whose band gaps are 3.31 and 3.34 eV. We all know that the optical properties of compounds are mainly determined by the electron transitions near the Fermi level. So, we focus on the atomic orbitals at the bottom of the conduction band (CB) and the top of the valence band (VB). The region from about −10 to 0 eV in the VBs is made up of electronic hybridization from the O 2p, P p, and Zn d states, and two nearly isolated peaks of alkaline metals are also found at the VBs (around −9 eV for RLZP and −7 eV for CLZP). The hybrid states from the O, Zn, and P atoms are also found at the bottom of the CBs.

The hybrid states come from the interaction among the P−O and Zn−O polyhedra, implying that these polyhedra are in dominant positions to determine the band gaps, refractive indices, and birefringences. The refractive indices and birefringences of RLZP and CLZP were further evaluated using the model structures shown in Figures 2 and S3. The obtained refractive indices of ordinary and extraordinary light and the anisotropic optical birefringence are shown in Figure 7. There are three different optical axes: $n_x > n_z > n_y$ for RLZP

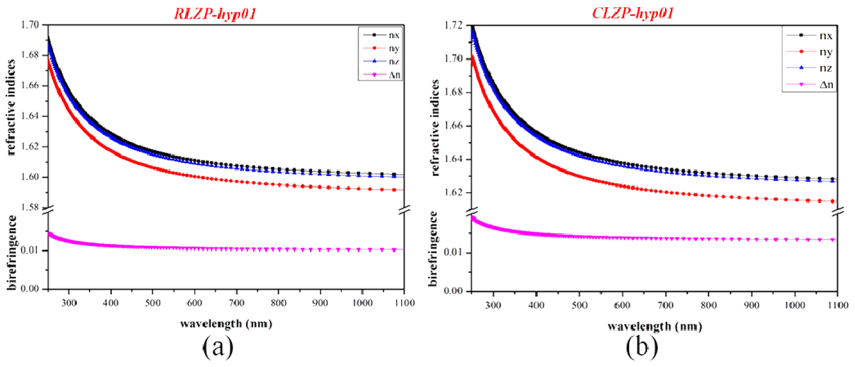

Figure 7. Obtained refractive indices and birefringences of (a) RLZP-hyp01 and (b) CLZP-hyp01.

DOI: 10.1021/acs.inorgchem.8b01140
Inorg. Chem. 2018, 57, 10568−10575

and CLZP, and the birefringences are very small (about 0.01 and 0.014 for RLZP and CLZP, respectively), which may relate to the unique P−O polyhedra. Some excellent phosphates with the P_2O_7 dimer also have low birefringence, such as $M_4Mg_4(P_2O_7)_3$ (M = K, Rb).[19]

CONCLUSION

In summary, a systematic investigation of the A_2O−ZnO−P_2O_5 (A = alkali metal) system produces two new phosphates: RLZP and CLZP. Contrasting the crystal structures reveals that both the ionic radius and interlayer spacing have an effect on the crystal configurations, and the ratios of M/P have an influence on the polymerization degree of the anionic groups. The title compounds possess experimental band gaps of 4.78 eV (RLZP) and 4.84 eV (CLZP), and the UV cutoff edges of both compounds are approximately 260 nm. The relationship between the electronic structures and optical properties is studied by theoretical calculations. According to the guidance of this work, we will continue to design phosphates with new structures and good optical properties in the follow-up research.

ASSOCIATED CONTENT

Supporting Information

The Supporting Information is available free of charge on the ACS Publications website at DOI: 10.1021/acs.inorgchem.8b01140.

Atomic coordinates (10^4) and equivalent isotropic displacement parameters ($\times 10^3$ Å^2) for RLZP and CLZP (U_{eq} is defined as one-third of the trace of the orthogonalized U_{ij} tensor), selected bond distances (Å) and angles (deg) for RLZP and CLZP, related bond distances (Å) and angles (deg) for P_2O_7 of KLZP and RLZP, powder XRD patterns of the title compounds before and after melting, photographs of the RLZP and CLZP crystals, models of CLZP used for first-principles calculations, 3D structure of CLZP and the CsO_{12} polyhedra composed of 1D chains along the *c* axis, P_2O_7 of $ALiZnP_2O_7$ (A = Na, K, Rb, Cs), IR spectra of RLZP and CLZP, and TG−DSC curves of RLZP and CLZP (PDF)

Accession Codes

CCDC 1840793−1840794 contain the supplementary crystallographic data for this paper. These data can be obtained free of charge via www.ccdc.cam.ac.uk/data_request/cif, or by emailing data_request@ccdc.cam.ac.uk, or by contacting The Cambridge Crystallographic Data Centre, 12 Union Road, Cambridge CB2 1EZ, UK; fax: +44 1223 336033.

AUTHOR INFORMATION

Corresponding Authors

*E-mail: chenzhaohui686@sina.cn (Z.C.). Phone: (86)-991-8582966. Fax: (86)-991-8582966.

*E-mail: qunjing@xju.edu.cn (Q.J.). Phone: (86)-991-8582966. Fax: (86)-991-8582966.

ORCID

Zhaohui Chen: 0000-0002-9472-2113

Qun Jing: 0000-0002-1801-2638

Author Contributions

‡These authors contributed equally to this work and should be considered cofirst authors.

Notes

The authors declare no competing financial interest.

ACKNOWLEDGMENTS

This work is supported by the National Natural Science Foundation of China (Grant 51462033), the Natural Science Foundation of Xinjiang Uygur Autonomous Region of China (Grant 2018D01C045), and the Science Research Projects in University of Xinjiang Education Department (Grant XJEDU2017M006).

REFERENCES

(1) (a) Yin, P.; Zheng, L. M.; Gao, S.; Xin, X. Q. Magnetic Properties of Metal Diphosphonate Compounds with One-Dimensional Chain Structures. *Chem. Mater.* **2003**, *15*, 3233−3236. (b) Mao, J. G. Structures and Luminescent Properties of Lanthanide Phosphonates. *Coord. Chem. Rev.* **2007**, *251*, 1493−1520. (c) Plabst, M.; McCusker, L. B.; Bein, T. Exceptional Ion-Exchange Selectivity in a Flexible Open Framework Lanthanum (III) Tetrakisphosphonate. *J. Am. Chem. Soc.* **2009**, *131*, 18112−18118. (d) Shi, X.; Zhu, G. S.; Qiu, S. L.; Huang, K. L.; Yu, J. H.; Xu, R. R. $Zn_2[(S)$-$O_3PCH_2NHC_4H_7CO_2]_2$: A Homochiral 3D Zinc Phosphonate with Helical Channels. *Angew. Chem., Int. Ed.* **2004**, *43*, 6482−6485. (e) Wang, D. Y.; Buqa, H.; Crouzet, M.; Deghenghi, G.; Drezen, T.; Exnar, I.; Kwon, N. H.; Miners, J. H.; Poletto, L.; Grätzel, M. High-Performance, Nano-Structured $LiMnPO_4$ Synthesized via a Polyol Method. *J. Power Sources* **2009**, *189*, 624−628. (f) Pan, S. L.; Wu, Y. C.; Fu, P. Z.; Zhang, G.; Li, Z.; Du, C.; Chen, C. Growth, Structure, and Properties of Single Crystals of $SrBPO_5$. *Chem. Mater.* **2003**, *15*, 2218−2221. (g) Liu, W.; Ge, M.; Yang, X.; Chen, H.; Li, M.; Zhao, J. Hydrothermal Synthesis and Characterization of Two Organically Templated Cadmium Borophosphates with Novel Structures. *Inorg. Chem.* **2004**, *43*, 3910−3914. (h) Zhang, S.; Huang, Y.; Seo, H. J. Luminescence Properties and Structure of Eu^{2+} Doped $KMgPO_4$ Phosphor. *Opt. Mater.* **2010**, *32*, 1545−1548.

(2) (a) Padhi, A. K.; Nanjundaswamy, K. S.; Goodenough, J. B. D. Phospho-Olivines as Positive-Electrode Materials for Rechargeable Lithium Batteries. *J. Electrochem. Soc.* **1997**, *144*, 1188−1194. (b) Huang, H.; Yin, S. C.; Kerr, T.; Taylor, N.; Nazar, L. F. Nanostructured Composites: A High Capacity, Fast Rate-$Li_3V_2(PO_4)_3$/Carbon Cathode for Rechargeable Lithium Batteries. *Adv. Mater.* **2002**, *14*, 1525−1528.

(3) (a) Choi, S.; Yun, Y. J.; Jung, H. K. Eu^{2+} and Mn^{2+} Activated Single Phase White Emitting Phosphor $Na(Sr, Ba)PO_4$ for Phosphor Converted-LEDs. *Mater. Lett.* **2012**, *75*, 186−188. (b) Im, W. B.; Yoo, H. S.; Vaidyanathan, S.; Kwon, K. H.; Park, H. J.; Kim, Y. I.; Jeon, D. Y. A Novel Blue-Emitting Silica-Coated $KBaPO_4$:Eu^{2+} Phosphor under Vacuum Ultraviolet and Ultraviolet Excitation. *Mater. Chem. Phys.* **2009**, *115*, 161−164. (c) Huang, Y. L.; Seo, H. J. Luminescence of Eu^{2+} Ions in $CsMgPO_4$ Phosphor: Anomalous Emission and Its Origin. *J. Electrochem. Soc.* **2011**, *158*, J260−J263. (d) Song, H. J.; Yim, D. K.; Roh, H. S.; Cho, I. S.; Kim, S. J.; Jin, Y. H.; Shim, H. W.; Kim, D. W.; Hong, K. S. $RbBaPO_4$: Eu^{2+}: A New Alternative Blue-Emitting Phosphor for UV-Based White Light-Emitting Diodes. *J. Mater. Chem. C* **2013**, *1*, 500−505.

(4) (a) Wang, Y.; Pan, S. L.; Su, X.; Yang, Z. H.; Dong, L. Y.; Zhang, M. New Molybdenum (VI) Phosphates: Synthesis, Characterization, and Calculations of Centrosymmetric $RbMoO_2PO_4$ and Non-centrosymmetric $Rb_4Mo_5P_2O_{22}$. *Inorg. Chem.* **2013**, *52*, 1488−1495. (b) Li, L.; Han, S. J.; Lei, B. H.; Wang, Y.; Li, H. Y.; Yang, Z. H.; Pan, S. L. Three New Phosphates with Isolated P_2O_7 Units: Non-centrosymmetric $Cs_2Ba_3(P_2O_7)_2$ and Centrosymmetric $Cs_2BaP_2O_7$ and $LiCsBaP_2O_7$. *Dalton Trans.* **2016**, *45*, 3936−3942. (c) Abudoureheman, M.; Han, S. J.; Lei, B. H.; Yang, Z. H.; Long, X. F.; Pan, S. L. $KPb_2(PO_3)_5$: A Novel Nonlinear Optical Lead Polyphosphate with a Short Deep-UV Cutoff Edge. *J. Mater. Chem. C* **2016**, *4*, 10630−10637. (d) Sun, T. Q.; Shan, P.; Chen, H.; Liu, X. W.; Liu, H. D.; Chen, S. L.; Cao, Y. A.; Kong, Y. F.; Xu, J. J. Growth and Properties of

DOI: 10.1021/acs.inorgchem.8b01140
Inorg. Chem. 2018, 57, 10568−10575

a Noncentrosymmetric Polyphosphate $CsLa(PO_3)_4$ Crystal with Deep-Ultraviolet Transparency. *CrystEngComm* **2014**, *16*, 10497−10504.
(5) Yu, P.; Wu, L. M.; Zhou, L. J.; Chen, L. Deep-Ultraviolet Nonlinear Optical Crystals: $Ba_3P_3O_{10}X$ (X= Cl, Br). *J. Am. Chem. Soc.* **2014**, *136*, 480−487.
(6) He, R.; Huang, H. W.; Kang, L.; Yao, W. J.; Jiang, X. X.; Lin, Z. S.; Qin, J. G.; Chen, C. T. Bandgaps in the Deep Ultraviolet Borate Crystals: Prediction and Improvement. *Appl. Phys. Lett.* **2013**, *102*, 231904.
(7) (a) Li, L.; Wang, Y.; Lei, B. H.; Han, S. J.; Yang, Z. H.; Poeppelmeier, K. R.; Pan, S. L. A New Deep-Ultraviolet Transparent Orthophosphate $LiCs_2PO_4$ with Large Second Harmonic Generation Response. *J. Am. Chem. Soc.* **2016**, *138*, 9101−9104. (b) Shen, Y. G.; Yang, Y.; Zhao, S. G.; Zhao, B. Q.; Lin, Z. S.; Ji, C. M.; Li, L.; Fu, P.; Hong, M. C.; Luo, J. H. Deep-Ultraviolet Transparent Cs_2LiPO_4 Exhibits an Unprecedented Second Harmonic Generation. *Chem. Mater.* **2016**, *28*, 7110−7116. (c) Cheng, X. Y.; Whangbo, M. H.; Guo, G. C.; Hong, M. C.; Deng, S. Q. The Large Second-Harmonic Generation of $LiCs_2PO_4$ is Caused by the Metal-Cation-Centered Groups. *Angew. Chem., Int. Ed.* **2018**, *57*, 3933−3937. (d) Zhao, S. G.; Gong, P. F.; Luo, S. Y.; Bai, L.; Lin, Z. S.; Tang, Y. Y.; Zhou, Y. L.; Hong, M. C.; Luo, J. H. Tailored Synthesis of a Nonlinear Optical Phosphate with a Short Absorption Edge. *Angew. Chem., Int. Ed.* **2015**, *54*, 4217−4221. (e) Zhao, S. G.; Gong, P. F.; Luo, S. Y.; Bai, L.; Lin, Z. S.; Ji, C. M.; Chen, T. L.; Hong, M. C.; Luo, J. H. Deep-Ultraviolet Transparent Phosphates $RbBa_2(PO_3)_5$ and $Rb_2Ba_3(P_2O_7)_2$ Show Nonlinear Optical Activity from Condensation of $[PO_4]^{3-}$ Units. *J. Am. Chem. Soc.* **2014**, *136*, 8560−8563. (f) Shan, P.; Sun, T. Q.; Chen, H.; Liu, H. D.; Chen, S. L.; Liu, X. W.; Kong, Y. F.; Xu, J. J. Crystal Growth and Optical Characteristics of Beryllium-Free Polyphosphate, $KLa(PO_3)_4$, a Possible Deep-Ultraviolet Nonlinear Optical Crystal. *Sci. Rep.* **2016**, *6*, 25201−25211. (g) Zhao, S. G.; Yang, X. Y.; Yang, Y.; Kuang, X. J.; Lu, F. Q.; Shan, P.; Sun, Z. H.; Lin, Z. S.; Hong, M. C.; Luo, J. H. Non-Centrosymmetric $RbNaMgP_2O_7$ with Unprecedented Thermo-Induced Enhancement of Second Harmonic Generation. *J. Am. Chem. Soc.* **2018**, *140*, 1592−1595. (h) Zhao, S. G.; Yang, Y.; Shen, Y. G.; Wang, X. D.; Ding, Q. R.; Li, X. F.; Li, Y. Q.; Li, L.; Lin, Z. S.; Luo, J. H. Beryllium-free Deep-UV Nonlinear Optical Material $CsNaMgP_2O_7$ with Honeycomb-Like Topological Layers. *J. Mater. Chem. C* **2018**, *6*, 3910−3916.
(8) (a) Abudoureheman, M.; Han, S. J.; Wang, Y.; Lei, B. H.; Yang, Z. H.; Pan, S. L. $A_3Sr_2P_7O_{21}$ (A = Rb, Cs): Two Polyphosphates Based on Different Types of P−O Chains and Ring Structures. *Inorg. Chem.* **2017**, *56*, 3939−3945. (b) Chen, Y. G.; Xing, M. L.; Liu, P. F.; Guo, Y.; Yang, N.; Zhang, X. M. Two Phosphates: Noncentrosymmetric $Cs_6Mg_6(PO_3)_{18}$ and Centrosymmetric $Cs_2MgZn_2(P_2O_7)_2$. *Inorg. Chem.* **2017**, *56*, 845−851. (c) Zhang, X. Y.; Wu, H. P.; Wang, Y.; Dong, X. Y.; Han, S. J.; Pan, S. L. Application of the Dimensional Reduction Formalism to $Pb_{12}[Li_2(P_2O_7)_2(P_4O_{13})_2]$-$(P_4O_{13})$: A Phosphate Containing Three Types of Isolated P−O Groups. *Inorg. Chem.* **2016**, *55*, 7329−7331.
(9) Lapshin, A. E.; Petrova, M. A. Mixed Alkali Zinc Diphosphates: Synthesis, Structure, and Properties. *Glass Phys. Chem.* **2012**, *38*, 491−503.
(10) (a) Shepelev, Yu. F.; Lapshin, A. E.; Petrova, M. A.; Novikova, A. S. Crystal Structure of the $LiNaZnP_2O_7$ Compound in the $Li_2ZnP_2O_7$−$Na_2ZnP_2O_7$ Glass-Forming System. *Glass Phys. Chem.* **2005**, *31*, 690−693. (b) Shepelev, Y. F.; Lapshin, A. E.; Petrova, M. A. Crystal Structure of Sodium Potassium Zinc Diphosphate NaKZn-P_2O_7. *J. Struct. Chem.* **2006**, *47*, 1098−1102. (c) Shepelev, Yu. F.; Petrova, M. A.; Novikova, A. S.; Lapshin, A. E. Crystal Structures of $Na_2ZnP_2O_7$, $K_2ZnP_2O_7$, and $LiKZnP_2O_7$ Phases in the M_2O−ZnO−P_2O_5 Glass-Forming System (M = Li, Na, and K). *Glass Phys. Chem.* **2002**, *28*, 317−321.
(11) *SAINT-Plus*, version 6.02A; Bruker Analytical X-ray Instruments, Inc.: Madison, WI, 2000.
(12) Sheldrick, G. M. *SHELXTL*, version 6.14; Bruker Analytical Xray Instruments, Inc.: Madison, WI, 2004.
(13) Spek, A. L. Single-Crystal Structure Validation with the Program PLATON. *J. Appl. Crystallogr.* **2003**, *36*, 7.
(14) Clark, S. J.; Segall, M. D.; Pickard, C. J.; Hasnip, P. J.; Probert, M. J.; Refson, K.; Payne, M. C. First Principles Methods Using CASTEP. Z. *Z. Kristallogr. - Cryst. Mater.* **2005**, *220*, 567−572.
(15) Perdew, J.; Burke, K.; Ernzerhof, M. Generalized Gradient Approximation Made Simple. *Phys. Rev. Lett.* **1996**, *77*, 3865.
(16) (a) Shi, Y. J.; Wang, Y.; Pan, S. L.; Yang, Z. H.; Dong, X. Y.; Wu, H. P.; Zhang, M.; Cao, J.; Zhou, Z. X. Synthesis, Crystal Structures and Optical Properties of Two Congruent-Melting Isotypic Diphosphates: $LiM_3P_2O_7$ (M = Na, K). *J. Solid State Chem.* **2013**, *197*, 128−133. (b) Dong, X. Y.; Shi, Y. J.; Zhang, M. J.; Chen, Z. H.; Jing, Q.; Yang, Y.; Pan, S. L.; Yang, Z. H.; Li, H. Y. The Flexibility of P_2O_7 Dimers in Soft Structures: $M_2CdP_2O_7$ (M = Rb, Cs). *Eur. J. Inorg. Chem.* **2016**, *2016*, 2704−2708. (c) Shen, Y. G.; Zhao, S. G.; Zhao, B. Q.; Ji, C. M.; Li, L.; Sun, Z. H.; Hong, M. C.; Luo, J. H. Strong Nonlinear-Optical Response in the Pyrophosphate $CsLiCdP_2O_7$ with a Short Cutoff Edge. *Inorg. Chem.* **2016**, *55*, 11626−11629. (d) Ma, R. R.; Yang, Y.; Pan, S. L.; Sun, Y.; Yang, Z. Y. Structure Comparison and Optical Properties of $Na_7Mg_{4.5}(P_2O_7)_4$: A Sodium Magnesium Phosphate with Isolated P_2O_7 Units. *New J. Chem.* **2017**, *41*, 3399−3404. (e) Fang, Y.; Chen, Z. H.; Shi, Y. J.; Zhang, W. Y.; Dong, X. Y. $Li_{1.52}Na_{4.48}Cd_8(PO_4)_2(P_2O_7)_4$: A New Mixed-Anion Diphosphate Containing Four Types of Dimensions Groups. *Inorg. Chem. Commun.* **2017**, *86*, 253−257. (f) Falah, C.; Boughzala, H.; Jouini, T. Preparation and the Crystal Structure of Non-centrosymmetric $K_6Bi_2(P_2O_7)_3$. *Anal. Sci.* **2004**, *20*, 17−18. (g) Zhang, X. Y.; Wu, H. P.; Liu, Q.; Dong, X. Y.; Chen, Y. L.; Yang, Z. H.; Wen, X. D.; Pan, S. L. Application of the Dimensional Reduction Formalism to $Pb_{9-x}Ba_x[Li_2(P_2O_7)_2(P_4O_{13})_2]$ (x = 0, 2, 6, 7): A Series of Phosphates with Two Types of Isolated Polyphosphate Groups. *Dalton Trans.* **2017**, *46*, 4678−4684.
(17) Guo, F. J.; Hu, C.; Wang, Y.; Han, J.; Yang, Z. H.; Pan, S. L. Insights of BO_3−PO_4 Replacement for the Design and Synthesis of a New Borate-Phosphate with Unique $^1{}_\infty[Zn_4BO_{11}]$ Chains and Two New Phosphates. *Inorg. Chem. Front.* **2018**, *5*, 327−334.
(18) (a) Kubelka, P.; Munk, F. Z. Ein Beitrag Zur Optik Der Farbanstriche. *Z. Technol. Phys.* **1931**, *12*, 593. (b) Tauc, J. *Mater. Res. Bull.* **1970**, *5*, 721.
(19) Yu, H. W.; Young, J.; Wu, H. P.; Zhang, W. G.; Rondinelli, J. M.; Halasyamani, P. S. $M_4Mg_4(P_2O_7)_3$ (M = K, Rb): Structural Engineering of Pyrophosphates for Nonlinear Optical Applications. *Chem. Mater.* **2017**, *29*, 1845−1855.

DOI: 10.1021/acs.inorgchem.8b01140
Inorg. Chem. 2018, 57, 10568−10575